A Bayesian Adaptive Smoothing and Thresholding Approach for Activation Detection in Single-Subject fMRI

Juan Esteban Flórez Coronel

University of Puerto Rico, Mayaguez
Department of Mathematical Sciences

Advisor: Israel Almodóvar-Rivera, Ph.D.

June 25, 2024

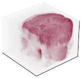

Contents

Contents

- **A%** activation percentage. 13, 29, 48, 51, 52, 54
- **AST** Adaptive Smoothing and Thresholding. 11, 13
- **BOLD** Blood Oxygenation Level-Dependent. 8, 16, 34, 38
- **CNR** Contrast-to-Noise Ratio. 38, 41–43, 48
- **fMRI** Functional Magnetic Resonance Imaging. 7, 13, 18, 32, 38, 54
- **FPR** False Positive Rate. 48, 51, 52
- **JI** Jaccard Index. 23, 48–52
- **SNR** Signal-to-Noise Ratio. 38, 41–43, 48
- **TN** Truncated Normal. 21, 25

Contents

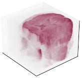

Contents

What is fMRI?

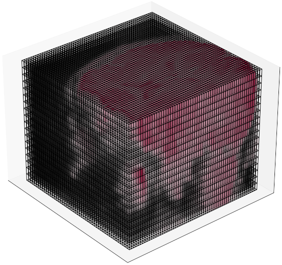

Figure 1: Voxels in fMRI Image

- Functional Magnetic Resonance Imaging (fMRI) is a non-invasive technique that take a series of MRI captures in a certain period of time to analyze the behavior of the studied body part in the elapsed time, normally, the body part is stimulated to study its effect [1].
- In fMRI, the brain image is divided into 3D unit volumes called voxels, typically, more than 10^5 per image.

BOLD

- The most common technique to generate images is the Blood Oxygenation Level-Dependent (BOLD).
- BOLD measures the local changes in deoxyhemoglobin concentration in the brain.
- The change in oxygenation produces different local magnetic fields.

Hemodynamic Response Function

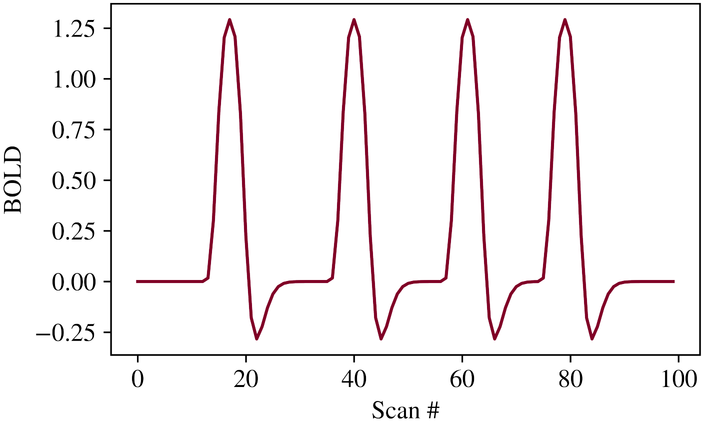

Figure 2: Glover Hemodynamic Response Function

Contents

Previous Works

- Identification of brain regions involved in language processing, memory, and decision-making [2, 3, 4].
- Identification of brain regions that are activated in response to specific stimuli or task [5, 6, 7].
- Methods used include time-series analysis, statistical parametric mapping, multivariate pattern classification, Bayesian modeling, among others [8, 9, 10, 11].
- Adaptive Smoothing and Thresholding (AST) method is also used by several researchers [12, 13, 14, 15].

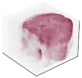

Contents

Objectives

- Perform Bayesian time-series analysis to obtain a posterior probability map of an fMRI image for a single-subject situation.
- Develop an AST method that inputs the probability posterior map and finds the possible activated voxels.
- Study the proposed algorithm in different simulation frameworks. Study the results in terms of similarity, rate of false positives, and activation percentage (A%).
- Finally, apply the algorithm to a real dataset.

Contents

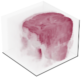

Contents

Time Series Model

- Each voxel has a time series associated to it.
- Let $\boldsymbol{y}_i$ be the response variable of the ith voxel, $\boldsymbol{X}$ be the design matrix of the study containing the expected BOLD change and β_i be the coefficient that contains the stimulus, then:

$$\boldsymbol{y}_i \sim N\left(\boldsymbol{X}\beta_i, \boldsymbol{\Sigma}\right)$$

- Note that $\boldsymbol{\Sigma}$ can have any structure, however, if we let $\boldsymbol{\Sigma} = \sigma^2 \boldsymbol{I}$, the independent model is obtained:

$$\boldsymbol{y}_i | \beta_i, \sigma, \boldsymbol{X} \sim N\left(\boldsymbol{X}\beta_i, \sigma^2 \boldsymbol{I}\right)$$

Bayesian Approach

- Using a noninformative prior distribution:

$$\pi\left(\beta_i, \sigma\right) \propto \frac{1}{\sigma^2}$$

- Using the Bayes' Rule and the ordinary least squares solution to a linear problem $\hat{\beta}_i = \left(\boldsymbol{X}^T\boldsymbol{X}\right)^{-1}\boldsymbol{X}^T\boldsymbol{y}_i$, the conditional posterior of β_i, given σ is then:

$$\pi\left(\beta_i | \sigma, \boldsymbol{y}_i\right) \sim N\left(\hat{\beta}_i, \left(\boldsymbol{X}^T\boldsymbol{X}\right)^{-1}\sigma^2\right).$$

Posterior Probability Maps

- Now, for each voxel, i, in the region of interest of our study, calculate the posterior probability that the coefficient associated with the stimulus, t, is not zero, which is roughly estimated using:

$$P(\beta_{i,t} > 0 | \boldsymbol{y}_i, \boldsymbol{X}).$$

- Let $\mathbb{P} = \{P(\beta_{i,t} > 0 | \boldsymbol{y}_i, \boldsymbol{X})\}_{i=[1,v]}$ represent a Posterior Probability Map, where v is the number of voxels in the region of interest of an fMRI experiment.

Posterior Probability Map

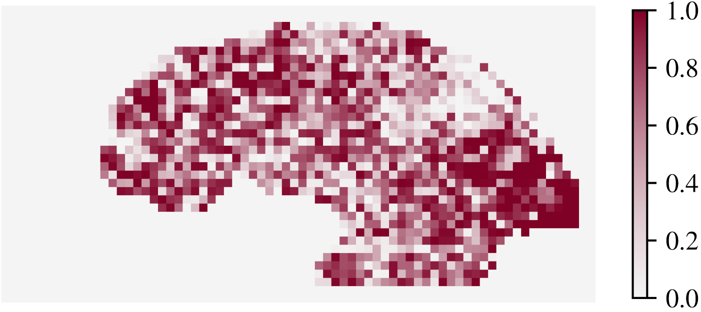

Figure 3: Example of a Posterior Probability Map

Contents

Relevant Distributions

- We will study $\mathbb{P}$ as a Truncated Normal (TN) Distribution in the interval $[0, 1]$.
- $TN(0, 1)$ is in the domain of maximal attraction of the limiting distribution G, a Gumbel distribution.
  - Therefore, $TN^v(a_v x + b_v) \to G(x)$.
  - For $a_v = [v\psi(b_v)]^{-1}$ and $b_v = \Psi^{-1}(1 - 1/v)$.
  - Where ψ and Ψ are the PDF and CDF of the TN, respectively.

Gaussian Kernel Smoothing

- Convolution of the image with:
  - Gaussian function in 2D: $G(x, y) = \frac{1}{2\pi\sigma_s^2} \exp\left(-\frac{x^2+y^2}{2\sigma_s^2}\right)$.
  - This can be extended to 3D.

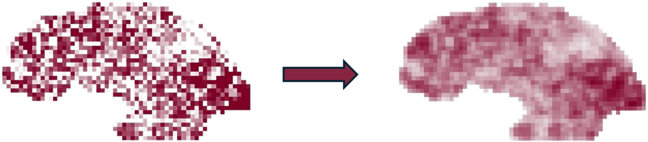

Figure 4: Example of the Smoothing Process in Posterior Probability Map

Jaccard Index (JI)

- Used to calculate image similarity:
  - $J(\boldsymbol{A}, \boldsymbol{B}) = \frac{|\boldsymbol{A} \cap \boldsymbol{B}|}{|\boldsymbol{A} \cup \boldsymbol{B}|}$

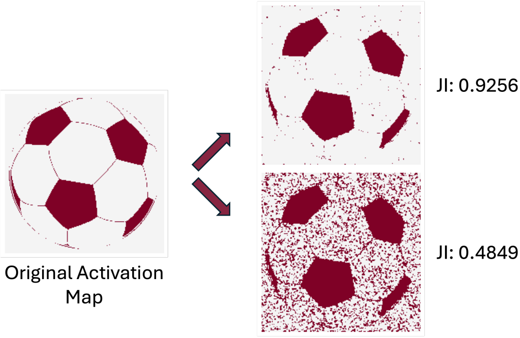

Figure 5: Example of Similarity Measurement Using JI

bFAST Algorithm

- Initialization
  - $\mathbb{P}^{\mathbf{(0)}} = \mathbb{P}$
  - $\zeta_i \equiv 0 \forall i$, where ζ_i is 1 when voxel i is activated and 0 if not.
  - $\zeta_i^{(0)} \equiv \zeta_i$
  - $v_0 = v$, where v_k is the number of voxels for which $\zeta_i^{(k)} = 0$.

bFAST Algorithm

- For $k = 1, 2, \ldots,$ iterate as follows:
  - *Smoothing*. Smooth $\mathbb{P}^{\boldsymbol{(k-1)}}$ using a Gaussian Kernel to obtain $\mathbb{P}^{\boldsymbol{(k)}}$. Let $\sigma_s = 0.65 + 100(k-1)$.
  - *Thresholding*. This consists of three steps:
    - Estimate $\mathbb{P}^{\boldsymbol{(k-1)}}$ as a TN.
    - Calculate a_v and b_v.
    - Calculate the probability threshold, $\eta = a_v \iota_{0.01} + b_v$, with $\iota_{0.01}$ be the upper-tail 0.01-value of the standard Gumbel Distribution.
  - *Activation*: Set $\zeta_i^{(k)} = 1$ if $\zeta_i^{(k-1)} = 0$ and the value of the ith voxel of $\mathbb{P}^{\boldsymbol{(k)}}$ is greater than η. Calculate $v_k = \sum_{i=1}^{v} \zeta_i^{(k)}$.

bFAST Algorithm

- Termination
  - Declare no activation and terminate if $\zeta^{(1)} \equiv 0$.
  - If $J(\zeta^{(k)}, \zeta^{(k-1)}) \geq J(\zeta^{(k+1)}, \zeta^{(k)})$, the algorithm terminates and the final activation map is $\zeta^{(k)}$.
  - The maximum number of iterations is default to $k = 10$.

Contents

Contents

True Maps Summary

Table 1: Details of True Maps Considered. In both maps, dark voxels are active and light voxels are inactive.

Name	2D	3D
Dimensions	200×200	$40 \times 40 \times 25$
Voxels	40000	40000
A%	19.9375	3.9525
Map	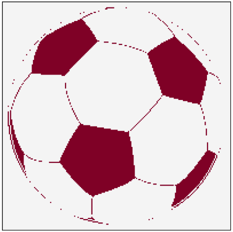	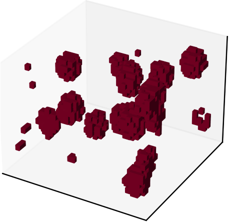

3D Map Creation

- Step 1. Create a random 40×40 grid of numbers between 0 and 1. The ones that are greater than 0.99 take a value of 1, the rest are 0.
- Step 2. For each of those ones, select a random integer between 1 and 25 to be the depth of the cluster in the 3D grid.
- Step 3. At each of the cluster centers, generate a ball of radius 5. For each voxel inside that ball, randomly mark as active only the 67% of them.
- Step 4. Identify inactive voxels in each cluster that are surrounded by at least 4 active voxels. If so, mark it as active.

Contents

Design Matrix

- $\boldsymbol{X}$ will consist of 2 columns and one row per scan.
- The second column corresponds to the constant regressor.
- The first column contains the Glover Hemodynamic Response Function given the following event description:

Table 2: Event Description of Simulated fMRI Experiment

Parameter	**Value**
Number of Scans	100
Time Between Scans	2 seconds
Number of Stimulus	4
Duration of Each Stimulus	10 seconds
Time Between Stimulus	18 - 25 seconds

Contents

BOLD

- BOLD response without noise is computed depending on the voxel activation status, ζ_i, on the true map. See Table 3.

Table 3: Parameter Selection Based on Activation Status

Activation Status	**Parameter Values**
$\zeta_i = 0$	$\beta_i^* = (0, 100)^T$
$\zeta_i = 1$	$\beta_i^* = (75, 100)^T$

- BOLD response, $\boldsymbol{y}_i$, for each voxel i depends on the BOLD response without noise, $\boldsymbol{X}\beta_i^*$, and the noise generated using an *ARMA* Model, $\boldsymbol{\epsilon}$:

$$\boldsymbol{y}_i = \boldsymbol{X}\beta_i^* + \boldsymbol{\epsilon}.$$

Contents

Noise with ARMA

- The noise (ϵ) is a vector of mean $\mu = 0$ and variance $\sigma^2 = 25^2$ with a baseline structure equivalent to:

$$ARMA_{\epsilon}\left(\{p_1, p_2, \ldots\}, \{q_1, q_2, \ldots\}\right).$$

- $p = |\{p_1, p_2, \ldots\}|$ and $q = |\{q_1, q_2, \ldots\}|$ are related to the order of the corresponding $ARMA$ model, where p_a and q_b represent the coefficients of such models.
- $p, q \in [0, 1, 2, 3]$ were chosen to study the model under different noise scenarios. The values of p_a, and q_b were chosen arbitrarily as parameters. See Table 4.

Noise with ARMA

Table 4: Parameter Selection Related to ϵ

		p			
		0	1	2	3
q	0	$\{\},\{\}$	$\{\frac{1}{2}\},\{\}$	$\{\frac{1}{2},\frac{3}{10}\},\{\}$	$\{\frac{1}{2},\frac{3}{10},\frac{1}{10}\},\{\}$
	1	$\{\},\{\frac{1}{2}\}$	$\{\frac{1}{2}\},\{\frac{1}{2}\}$	$\{\frac{1}{2},\frac{3}{10}\},\{\frac{1}{2}\}$	$\{\frac{1}{2},\frac{3}{10},\frac{1}{10}\},\{\frac{1}{2}\}$
	2	$\{\},\{\frac{1}{2},\frac{3}{10}\}$	$\{\frac{1}{2}\},\{\frac{1}{2},\frac{3}{10}\}$	$\{\frac{1}{2},\frac{3}{10}\},\{\frac{1}{2},\frac{3}{10}\}$	$\{\frac{1}{2},\frac{3}{10},\frac{1}{10}\},\{\frac{1}{2},\frac{3}{10}\}$
	3	$\{\},\{\frac{1}{2},\frac{3}{10},\frac{1}{10}\}$	$\{\frac{1}{2}\},\{\frac{1}{2},\frac{3}{10},\frac{1}{10}\}$	$\{\frac{1}{2},\frac{3}{10}\},\{\frac{1}{2},\frac{3}{10},\frac{1}{10}\}$	$\{\frac{1}{2},\frac{3}{10},\frac{1}{10}\},\{\frac{1}{2},\frac{3}{10},\frac{1}{10}\}$

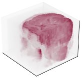

SNR and CNR

- Signal-to-Noise Ratio (SNR) represents how strong the signal is with respect to the noise.
  - Generally, the Signal-to-Noise Ratio (SNR) value of an fMRI experiment is around 4.
- Contrast-to-Noise Ratio (CNR) represents how significant is the BOLD change in activation regions with respect to the noise.
  - Generally, the Contrast-to-Noise Ratio (CNR) value of an fMRI experiment is around 3.

Contents

Contents

Noise in Simulations

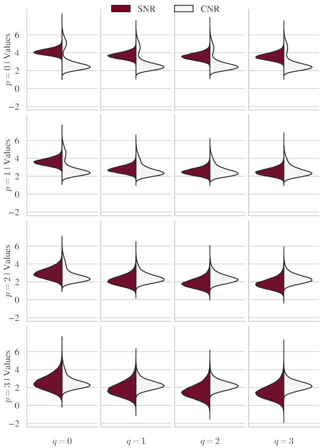

Figure 6: Numerical Distribution of the Voxel-Wise SNR and CNR Values of 2D Map

Noise in Simulations

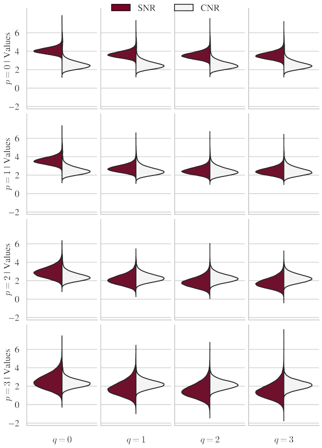

Figure 7: Numerical Distribution of the Voxel-Wise SNR and CNR Values of 3D Map

Noise in Simulations

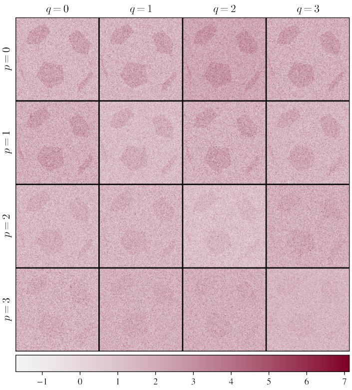

Figure 8: Spatial Distribution of the SNR Values in 2D Map

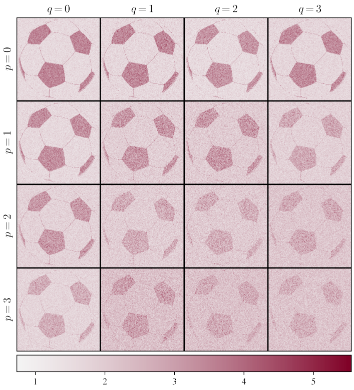

Figure 9: Spatial Distribution of the CNR Values in 2D Map

Contents

Example of bFAST Iterations

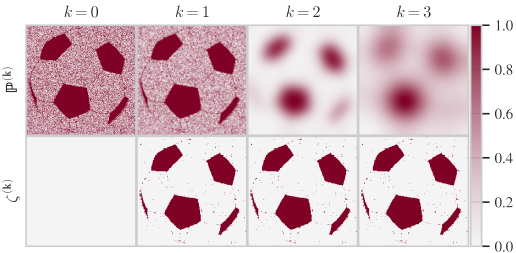

Figure 10: Example in 2D Map for $p, q = 0$

Example of bFAST Iterations

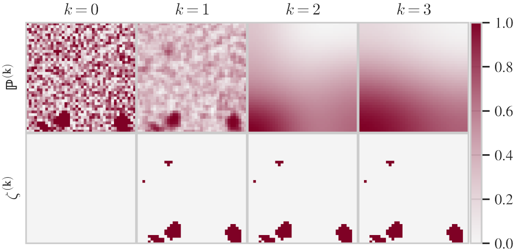

Figure 11: Example in $z = 20$ Plane of 3D Map for $p, q = 0$

Contents

Performance Metrics

- The performance of the bFAST algorithm was evaluated by comparing the final activation map with the true activation map using:
  - Jaccard Index (JI): Similarity between the two maps.
  - False Positive Rate (FPR): Ratio of the voxels marked as activated that are not really active and the total number of inactive voxels.
  - A%: Percentage of active voxels between both maps.
- Performance was evaluated in each of the noise scenarios considered and an average value for the SNR and CNR is also presented.

Performance Metrics

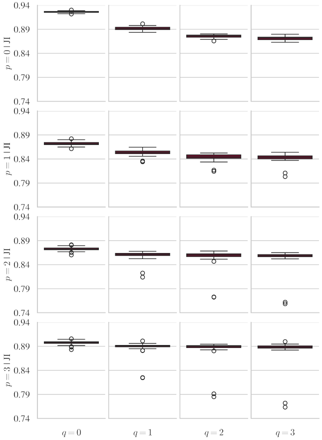

Figure 12: Jaccard Index in 2D Map

Performance Metrics

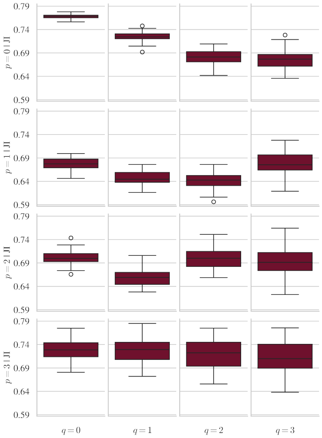

Figure 13: Jaccard Index in 3D Map

Performance Metrics

Table 5: Performance Metrics Summary in 2D Case

P	Q	SNR	CNR	JI	FPR	A%
0	0	4.0841	3.0344	0.9256	0.0078	19.663
	1	3.6815	2.9342	0.8925	0.0180	20.515
	2	3.5788	2.9035	0.8754	0.0227	20.858
	3	3.5688	2.8960	0.8695	0.0244	20.995
1	0	3.5988	2.9042	0.8794	0.0222	20.870
	1	2.7538	2.6993	0.8509	0.0299	21.398
	2	2.5159	2.6191	0.8488	0.0308	21.475
	3	2.4691	2.6007	0.8533	0.0292	21.350
2	0	2.9564	2.7050	0.8685	0.0240	20.908
	1	2.1686	2.4761	0.8648	0.0267	21.228
	2	1.8753	2.3861	0.8578	0.0284	21.333
	3	1.8050	2.3646	0.8581	0.0283	21.313
3	0	2.5794	2.5607	0.8932	0.0174	20.445
	1	1.8416	2.3420	0.8882	0.0185	20.513
	2	1.5895	2.2576	0.8837	0.0200	20.638
	3	1.5260	2.2323	0.8793	0.0213	20.740

Performance Metrics

Table 6: Performance Metrics Summary in 2D Case

P	Q	SNR	CNR	JI	FPR	A%
0	0	4.0430	2.6156	0.7677	0.0046	3.8075
	1	3.6401	2.5873	0.7249	0.0068	3.9950
	2	3.5348	2.5699	0.6796	0.0086	4.0675
	3	3.5233	2.5660	0.6767	0.0082	3.9950
1	0	3.5553	2.5687	0.6741	0.0092	4.1500
	1	2.7134	2.4836	0.6468	0.0108	4.2650
	2	2.4711	2.4406	0.6410	0.0116	4.3550
	3	2.4303	2.4320	0.6757	0.0099	4.2625
2	0	2.9143	2.4583	0.6979	0.0083	4.1125
	1	2.1205	2.3332	0.6566	0.0108	4.3100
	2	1.8440	2.2791	0.6909	0.0079	4.0075
	3	1.7735	2.2584	0.6859	0.0081	4.0300
3	0	2.5407	2.3554	0.7297	0.0065	3.9650
	1	1.8073	2.2290	0.7194	0.0067	3.9525
	2	1.5582	2.1729	0.7167	0.0074	4.0600
	3	1.5004	2.1515	0.7092	0.0066	3.8925

Contents

bFAST in Real Data

- Theory of Mind fMRI experiment by Moran (2012) [16].
- 48 participants, most of them in their 20's and some other in their 70's.
- Gradient-echo echo-planar pulse sequence on a 3T Tim Trio MRI scanner
- Stimulus are false belief question, false belief story, false photo question, and false photo story.
- Data has dimensions $72 \times 72 \times 36$ of 2 mm isotropic voxels.
- 40078 Voxels in the Region of Interest
- bFAST identified 1766 active voxels (4.41 A%) on the false belief question stimulus in the try 1 of subject 1.

bFAST in Real Data

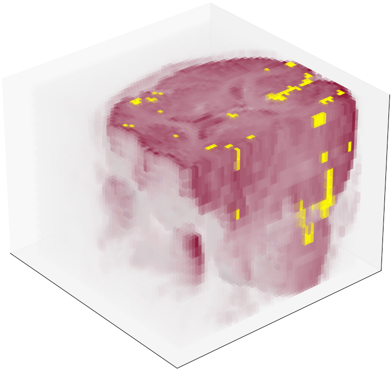

Figure 14: Activation Regions Identified by bFAST

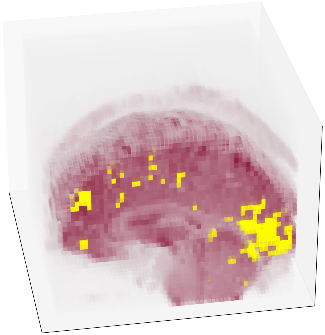

Figure 15: Activation Regions Identified by bFAST

Contents

References I

- B. R. Buchbinder, "Functional magnetic resonance imaging," *Handbook of clinical neurology*, vol. 135, pp. 61–92, 2016.
- W. D. Gaillard, B. C. Sachs, J. R. Whitnah, Z. Ahmad, L. M. Balsamo, J. R. Petrella, S. H. Braniecki, C. M. McKinney, K. Hunter, B. Xu, *et al.*, "Developmental aspects of language processing: fmri of verbal fluency in children and adults," *Human brain mapping*, vol. 18, no. 3, pp. 176–185, 2003.
- A. Golby, G. Silverberg, E. Race, S. Gabrieli, J. O'Shea, K. Knierim, G. Stebbins, and J. Gabrieli, "Memory encoding in alzheimer's disease: an fmri study of explicit and implicit memory," *Brain*, vol. 128, no. 4, pp. 773–787, 2005.

References II

- H. R. Heekeren, I. Wartenburger, H. Schmidt, H.-P. Schwintowski, and A. Villringer, "An fmri study of simple ethical decision-making," *Neuroreport*, vol. 14, no. 9, pp. 1215–1219, 2003.
- J. Orchard, C. Greif, G. H. Golub, B. Bjornson, and M. S. Atkins, "Simultaneous registration and activation detection for fmri," *IEEE transactions on medical imaging*, vol. 22, no. 11, pp. 1427–1435, 2003.
- T. Deneux and O. Faugeras, "Using nonlinear models in fmri data analysis: model selection and activation detection," *NeuroImage*, vol. 32, no. 4, pp. 1669–1689, 2006.

References III

- B. A. Ardekani, J. Kershaw, K. Kashikura, and I. Kanno, "Activation detection in functional mri using subspace modeling and maximum likelihood estimation," *IEEE Transactions on Medical Imaging*, vol. 18, no. 2, pp. 101–114, 1999.
- D. W. Adrian, R. Maitra, and D. B. Rowe, "Complex-valued time series modeling for improved activation detection in fmri studies," *The annals of applied statistics*, vol. 12, no. 3, p. 1451, 2018.
- J. Marchini and A. Presanis, "Comparing methods of analyzing fmri statistical parametric maps," *Neuroimage*, vol. 22, no. 3, pp. 1203–1213, 2004.

References IV

- J. A. Mumford, B. O. Turner, F. G. Ashby, and R. A. Poldrack, "Deconvolving bold activation in event-related designs for multivoxel pattern classification analyses," *Neuroimage*, vol. 59, no. 3, pp. 2636–2643, 2012.
- S. Makni, J. Idier, T. Vincent, B. Thirion, G. Dehaene-Lambertz, and P. Ciuciu, "A fully bayesian approach to the parcel-based detection-estimation of brain activity in fmri," *Neuroimage*, vol. 41, no. 3, pp. 941–969, 2008.
- K. Tabelow, J. Polzehl, H. U. Voss, and V. Spokoiny, "Analyzing fmri experiments with structural adaptive smoothing procedures," *NeuroImage*, vol. 33, no. 1, pp. 55–62, 2006.

References V

- M. A. Lindquist, J. M. Loh, and Y. R. Yue, "Adaptive spatial smoothing of fmri images," *Statistics and its Interface*, vol. 3, no. 1, pp. 3–13, 2010.
- F. Strappini, E. Gilboa, S. Pitzalis, K. Kay, M. McAvoy, A. Nehorai, and A. Z. Snyder, "Adaptive smoothing based on gaussian processes regression increases the sensitivity and specificity of fmri data," *Human brain mapping*, vol. 38, no. 3, pp. 1438–1459, 2017.
- I. Almodóvar-Rivera and R. Maitra, "Fast adaptive smoothing and thresholding for improved activation detection in low-signal fmri," *IEEE Transactions on Medical Imaging*, vol. 38, no. 12, pp. 2821–2828, 2019.

References VI

J. M. Moran, E. Jolly, and J. P. Mitchell, “Social-cognitive deficits in normal aging,” *Journal of neuroscience*, vol. 32, no. 16, pp. 5553–5561, 2012.